

Seasonal Contrasts in the Surface Energy Balance of the Sahel

R. L. Miller^{*,†}, A. Slingo[‡], J. C. Barnard[°], and E. Kassianov[°]

* Department of Applied Physics and Applied Math, Columbia University, New York, USA

† NASA Goddard Institute for Space Studies, New York, USA

‡ Environmental Systems Science Centre, University of Reading, Reading, UK

° Pacific Northwest National Laboratory, Richland, WA

To be submitted to *J. Geophys. Res.*

May 20, 2008

Abstract

Over most of the world ocean, heating of the surface by sunlight is balanced predominantly by evaporative cooling. Even over land, moisture for evaporation is available from vegetation or the soil reservoir. However, at the ARM Mobile Facility in Niamey, Niger, soil moisture is so depleted that evaporation makes a significant contribution to the surface energy balance only at the height of the rainy season, when precipitation has replenished the soil reservoir. Using observations at the Mobile Facility from late 2005 to early 2007, we describe how the surface balances radiative forcing. How the surface compensates time-averaged solar heating varies with seasonal changes in atmospheric water vapor, which modulates the greenhouse effect and the ability of the surface to radiate thermal energy directly to space. During the dry season, sunlight is balanced mainly by longwave radiation and the turbulent flux of sensible heat. The ability of longwave radiation to cool the surface drops after the onset of the West African summer monsoon, when moist, oceanic air flows onshore, increasing local column moisture and atmospheric opacity at these wavelengths. After the monsoon onset, but prior to significant rainfall, solar heating is compensated mainly by the sensible heat flux. During the rainy season, the magnitude of evaporation is initially controlled by the supply of moisture from precipitation. However, by the height of the rainy season, sufficient precipitation has accumulated at the surface that evaporation is related to the flux demanded by solar radiation, and radiative forcing of the surface is balanced comparably by the latent, sensible, and longwave fluxes. Radiative forcing of the surface also varies on a subseasonal time scale due to fluctuations in water vapor, clouds, and aerosol concentration. Except at the height of the rainy season, subseasonal forcing is balanced mainly by sensible heating and longwave anomalies. The efficacy of the sensible heat flux depends upon a positive feedback, where forcing changes mixing within the boundary layer and amplifies the sensible heating anomaly. How the surface responds to radiative forcing is fundamental to the climate response to dust and carbonaceous aerosols.

1 Introduction

To maintain thermal equilibrium, Earth must balance absorbed solar radiation with an equal outward flux at thermal wavelengths. At the surface of the planet, however, solar heating is offset mainly through evaporation rather than thermal radiation. Over most regions, upward thermal radiation from the surface is trapped by greenhouse absorbers, chief among them water vapor and clouds, followed by gases like carbon dioxide (*Kiehl and Trenberth, 1997*). Part of the absorbed flux is reradiated downward so that cooling of the surface by the net upward thermal flux is inefficient compared to evaporation (*Ravel and Ramanathan, 1989*). Surface evaporation is especially important within the tropical oceans (*Liu et al., 1994*), and even over land where moisture is available from vegetation or the soil reservoir.

However, at the Atmospheric Radiation Measurement (ARM) Mobile Facility in Niamey, Niger, a semi-arid region within the Sahel of western Africa, soil moisture is so depleted that solar heating is balanced mainly by longwave radiation and the turbulent flux of sensible heat. Evaporation makes a significant contribution to the surface energy balance only near the height of the rainy season, when precipitation has replenished the soil reservoir.

At Niamey, the sun is often obscured by aerosols, which are created by burning of vegetation, along with wind erosion of arid soils within the Sahel and Sahara (*Slingo et al., 2006; Johnson et al., 2008*). Sunlight is reduced beneath the aerosol layer as a result of absorption and reflection back to space (*Fouquart et al., 1987*), while the aerosol layer emits longwave radiation back toward the surface (*Guedalia et al., 1984*). The climate response to aerosols depends upon how the surface responds to the radiative perturbation, which is generally negative (*Miller and Tegen, 1998*). A reduction in the latent heat flux beneath the aerosol layer ultimately reduces precipitation (*Coakley and Cess, 1985; Miller and Tegen, 1998*), although radiative heating within the aerosol layer may induce ascent and cause a local increase in rainfall (*Miller et al., 2004b*). A reduction in the sensible heat flux decreases the vigor of boundary layer mixing. This reduces the magnitude of wind gusts associated with boundary layer eddies, along with the mixing of momentum down to the surface. Both effects reduce the surface wind speed, which impedes the lifting of additional soil particles into the atmosphere (*Miller et al., 2004a*).

The ARM Mobile Facility at Niamey is distinguished by its measurement of the entire suite of surface fluxes over a full seasonal cycle (*Miller and Slingo, 2007*). Because of the large aerosol burden throughout the year, it is an ideal location to examine how the climate responds to aerosol radiative forcing at the surface. As a preliminary study, we consider in this article how the response of surface energy fluxes to incident sunlight varies seasonally. Using measurements at the Mobile Facility from late 2005 to the early 2007, we examine how variations in sunlight incident upon the surface are balanced, both on seasonal and shorter time scales.

In Section 2, we describe the measurements used to characterize the seasonal cycle. In Section 3, we show that sunlight incident upon the surface is balanced differently according to the phase of the West African monsoon. In Section 4, we consider the surface response to subseasonal fluctuations of solar heating. We show that the cooling efficiency of longwave radiation drops after the onset of the summer monsoon, when moist, oceanic air flows on-shore, increasing local column moisture and atmospheric opacity at these wavelengths. Solar variations are balanced increasingly by turbulent fluxes, including evaporation, during this period. Our conclusions are given in Section 5.

2 Measurements

The ARM Mobile Facility was deployed at the airport in Niamey, Niger (2.18°E, 13.48°N) between November 2005 and January 2007. A complete description of the instrumentation is given by *Miller and Slingo* (2007). Here we describe the instruments that provide data analyzed in this study, listed in Table 1.

The surface energy budget consists of turbulent and radiative fluxes. Turbulent fluxes of latent and sensible heat were calculated using an eddy correlation system, which computes means and covariances of wind speed, temperature, and water vapor measured over a thirty minute period. Downwelling shortwave and longwave radiation were measured every minute by broadband radiometers. Upwelling fluxes were measured 2 m above the surface at the same temporal frequency. The downwelling longwave flux was measured independently by a second instrument, and the difference provides a measure of the uncertainty of each estimate. Over the fourteen months of the experiment, the root-mean-square difference was 3.6 Wm^{-2} , which was largest typically during mid-morning and mid-afternoon. The root-mean-square difference of the diurnal cycle was 0.8 Wm^{-2} . These are small compared to daily anomalies of downwelling longwave which are typically a few tens of Wm^{-2} during the dry season (November to April).

The net (or total) flux of heat into the surface departs from zero when averaged over a year, even if storage by the ground is neglected, because of individual biases in the instruments that measure the turbulent and radiative fluxes. As one measure of the precision of each flux, the net heat flux at the surface and its average imbalance over the course of the campaign were computed by summing the net solar and longwave fluxes together with the turbulent fluxes. To be consistent with the temporal resolution of the turbulent fluxes, the radiative fluxes were resampled every thirty minutes (after filtering periods shorter than sixty minutes to reduce aliasing). The net heat flux was computed at times when all of the separate turbulent and radiative fluxes were available, which during 2006 resulted in values for roughly 350 days, depending upon the time of day. The average imbalance of the net heat flux during 2006 was -6.5 Wm^{-2} . This value reflects measurement error (along with possible interannual variations in heat storage), but also the fact that slightly more observations

were available during the early afternoon (when the heating of the ground was largest) than around sunrise. If we form the average imbalance by averaging over the mean diurnal cycle (so that each time of day is equally represented), the average imbalance increases slightly to -6.6 Wm^{-2} . Either way, this imbalance is small compared to daily fluctuations in the individual turbulent and net solar and longwave fluxes, which are on the order of a few tens of Wm^{-2} .

In Section 4, we interpret variations in the surface radiative fluxes in terms of changes in atmospheric opacity related to water vapor, cloud cover, and the aerosol load. Water vapor within the atmospheric column was provided by Vaisalla RS-92 radiosondes. The sondes were launched four times daily at times clustered around 400, 1100, 1600, and 2330 local standard time. The column water was determined by summing over the depth of the sonde path, resulting in values that are comparable to the monthly averages retrieved by the NASA Water Vapor Project (NVAP; *Simpson et al.*, 2001). Column water vapor corresponding to individual sondes has a typical dry bias of less than 5% around noon, and a smaller wet bias at night compared to values derived from the Global Positioning System. These differences are small compared to daily averaged anomalies.

Aerosol optical thickness (AOT) was retrieved from measurements of the direct and diffuse solar flux at six wavelengths by the Multifilter Rotating Shadowband Radiometer (MFRSR; *McFarlane et al.*, 2008). Measurements are taken every 20 seconds during daylight hours, although retrieval of AOT is precluded by the presence of clouds. To interpret daily variations in the surface radiative fluxes during the dry season (Section 4), we form daily averages of the MFRSR retrieval of AOT at 500 nm. Without interpolation, clouds prevent the retrieval of AOT and the construction of a daily average roughly three days a month during the dry season, and between January 27 and February 18, eight daily averages are unavailable. Of the remaining days, daily averages are occasionally constructed from only a small number of retrievals, which introduces a sampling uncertainty. However, we found that daily averages of AOT retrieved from the MFRSR at the Mobile Facility in Niamey are highly correlated with the 440 nm AOT retrieved at the AERONET site at Banizoumbou, 50 km to the northeast. Correlations within a 15 day moving window are typically between

0.9 and 1.0 during the dry season, except during early February, when MFRSR retrievals of AOT are completely precluded by clouds on many days and the correlation falls to roughly 0.8. The high correlation suggests that aerosol variations occur over a broad spatial scale, encompassing both instrument sites, and that the MFRSR retrievals give a reliable estimate of daily averaged AOT, despite our interpolation and large day to day variations in the number of retrievals available.

Cloud optical thickness is retrieved by the International Satellite Cloud Climatology Project (ISCCP; *Rossow and Duenas, 2004*), using visible radiances measured by Meteosat every three hours. On 1 July 2006, midway through the AMF campaign at Niamey, the platform carrying the radiance instrument changed from Meteosat-7 to Meteosat-8. We formed a daily average of cloud optical thickness by combining DX retrievals of cloud optical thickness for the 30 km pixel encompassing Niamey at 9, 12, and 15 h local time. (Retrievals are not made at 6 and 18 h because of the low solar zenith angle.) Missing retrievals preclude the calculation of a daily average about three days a month. The retrieval of cloud optical thickness depends upon whether a water or ice cloud is detected, which is determined mainly by cloud top temperature.

Precipitation, measured using an optical instrument on a 10 m tower at the Mobile Facility, is used to interpret evaporative anomalies. The instrument continuously measures the interruption of an infrared beam by rainfall, archiving the total every minute. Precipitation was also measured using a conventional rain gauge roughly a kilometer away at another site at the Niamey airport (Hamidou Hama, personal communication). During 2006, the AMF recorded 37.6 cm of rainfall compared to 42.4 cm by the gauge (*Slingo et al., 2008a*). However, the near agreement of the annual totals is due to a single 20 minute event on the morning of 24 July, when 9.4 cm fell on the AMF instrument that was not recorded by the nearby gauge. In general, the AMF values are smaller compared to the gauge values than indicated by the annual total. Out of the roughly 180 day rainy season at Niamey, 52 days were identified as rainy by the AMF instrument compared to 57 days for the gauge (with a rainy day defined by an accumulation of at least 0.1 mm of rain), with 39 of these days in common. The overlap increases to roughly 45 days, if events around midnight are included

that were attributed to different days by the two instruments. For comparison, only 10 to 25 days would be in common if either instrument were identifying rainy days at random, suggesting that both instruments have skill (see Appendix). The AMF instrument was in better agreement than the gauge with respect to the 3-hourly rainfall retrieved from the blend of Tropical Rainfall Measuring Mission (TRMM) radar and microwave measurements along with outgoing longwave radiances (3B42 Version 6; *Huffman et al.*, 1997), according to a rank correlation test. However, this may simply indicate that the AMF and satellite instruments retrieve rainfall using variables that are highly correlated, and may not indicate increased reliability of the AMF instrument relative to the gauge. The persistent aerosol haze at Niamey throughout the campaign may have caused problems for the optical gauge (Kenneth Kehoe, personal communication), which was replaced by a second instrument during the middle of May 2006.

Unless noted, we exclude periods with missing measurements from our analysis.

3 Seasonal Cycle of the Surface Energy Balance

In this section, we describe the seasonal evolution of the surface energy balance in the context of the regional climate. A more extensive description of the climate and atmospheric variability measured during the deployment of the ARM Mobile Facility (AMF) in 2006 is provided by *Slingo et al.* (2008a).

At Niamey, the surface winds divide the year into two seasons (*Nicholson and Grist*, 2003). During the dry season, between November and April, the northeasterly Harmattan wind brings desert air to Niamey that eventually flows offshore toward the Atlantic ITCZ. Then, within a few weeks beginning in April, the surface wind reverses with the arrival of the West African summer monsoon. Until October, there is comparatively weak southwesterly flow bringing moist air from the Gulf of Guinea. The seasonal reversal of the circulation during the 2006 deployment of the AMF is illustrated by back-trajectories of air arriving at Niamey, calculated by *Slingo et al.* (2008a). At the latitude of Niamey, the monsoon rains typically begin in April (*Nicholson and Grist*, 2003). Monsoon rainfall was below normal during the AMF deployment in 2006, following anomalously high rainfall during the preceding year (*Slingo et al.*, 2008a).

Monsoon onset at Niamey is marked by an abrupt increase in column water vapor, measured from the four times daily radiosondes and integrated with respect to height, shown in Figure 1. Surface measurements of temperature T_s and specific humidity q_s indicate an abrupt and coincident increase in moist static energy (equal to $h = C_p T_s + L q_s$ where C_p is the specific heat of air and L is the latent heat of vaporization). High moist static energy at the surface indicates unstable air prone to convective ascent and rainfall (*Emanuel*, 1994). During 2006, the monsoon arrived on schedule, as clearly marked by the change in surface wind direction in late April (*Slingo et al.*, 2008a). However, despite the accompanying large values of moist static energy and column moisture, rainfall remained modest and sporadic for over two months until the middle of July (Fig. 2). The delay of rainfall despite the abrupt increase in surface moisture may be a consequence of the shallow leading edge of the monsoon layer as it penetrates and is overridden by dry air from the desert to the north (*Hastenrath and Lamb*, 1977). The entrainment of dry air above the shallow monsoon layer would quickly

reduce the buoyancy of convective parcels rising from the surface. In addition, *Geerts and Dejene* (2005) show that substantial reevaporation occurs beneath summertime convection within the Sahel, compared to other regions of tropical rainfall, as hydrometeors descend through dry air toward the surface. Both of these factors would limit rainfall measured at the surface, even though moist static energy of the surface air is largest immediately following monsoon onset (Figure 1). Both factors operate every year, however, and do not explain why the monsoon rainfall was sporadic and unusually delayed by two months after the reversal of the surface winds during 2006.

The increase of column moisture with the arrival of the monsoon alters the surface energy budget. The radiative and turbulent surface fluxes, along with their seasonal variation within the measurement campaign, are shown in Figure 4. Solar radiation at the top of the atmosphere varies with the seasonal evolution of the solar zenith angle. This angle is greatest in late April and August when the sun passes overhead, but its daily average peaks later as the day lengthens toward the summer solstice (e.g., *Hartman*, 1994). Solar radiation also varies inversely with the earth-sun distance, which is greatest in July. When these effects are taken together, the daily average of the TOA incident solar flux peaks in early May and is fairly steady until August. This seasonal variation at TOA is exhibited by the net downwelling solar flux at the surface (equal to the measured difference of the downwelling and upwelling solar fluxes). During the dry season, solar heating is largely balanced by the net flux of upward longwave radiation from the surface (equal to the measured difference of the upwelling and downwelling longwave fluxes). Over most of the Tropics, longwave radiation by the surface is typically absorbed by atmospheric water vapor and reradiated downward, resulting in a small net flux and inefficient cooling of the surface (*Pierrehumbert*, 1995). However, during the dry season, column moisture over the Sahel is small compared to neighboring tropical values, and as a result of the weak greenhouse effect, the surface can cool efficiently by radiating longwave. During this season, the turbulent flux of sensible heat is roughly half the longwave, while the flux of latent heat is effectively zero, in the absence of moisture in the upper layers of soil that was largely depleted following the previous rainy season.

With the arrival of monsoonal air in late April, the downward flux of longwave emitted by the atmosphere increases markedly (Figure 3), coincident with a threefold increase in column moisture. Consequently, the net upward longwave flux falls to the level of the sensible heat flux. Evaporation increases as the soil moisture is replenished by rainfall, and by late July the longwave, sensible, and latent heat fluxes are of comparable importance. Evaporation falls off quickly after the end of the rains in September. When the monsoon winds reverse in late October, indicated by a drop in moist static energy and column moisture (Figure 1), longwave radiation is reestablished as the predominant mechanism balancing absorbed sunlight.

In summary, the surface energy balance can be characterized by three distinct periods. During the dry season, greenhouse absorption by water vapor is small, and the surface cools efficiently by radiating directly to space. The second period follows the return of moist air associated with the summer monsoon, which makes the column comparatively opaque to longwave radiated by the surface, and the sensible heat flux increases to compensate. Finally, after the summer rains replenish the reservoir of soil moisture, the latent heat flux becomes of comparable importance. The contrast between the diurnal cycle of the surface energy balance during the dry season and the height of the rainy season, when soil moisture is sufficient to sustain evaporation, is shown in Figure 5. Throughout the year, the sensible heat flux at midday represents the largest instantaneous flux of heat from the surface into the atmosphere. However, longwave radiation remains significant during the night, accounting for its predominant total contribution to the surface energy balance during the dry season. Figure 5 shows that the longwave flux peaks slightly later in the day than the sensible heat flux. The longwave flux includes a contribution from atmospheric emission, which depends upon the air temperature and humidity. As the boundary layer expands during the day, entraining dry air from above, surface humidity drops and the column becomes more transparent to longwave emission by the surface. This accounts for the later peak of net upward longwave compared to the sensible heat flux in Figure 5.

The surface energy balance measured at the AMF in Niamey, along with its seasonal evolution, appears to be typical of the Sahel, as indicated by previous measurement campaigns over a variety of land surfaces, including savannah, natural forest, and fields cultivated with

millet. *Wallace et al.* (1993) and *Verhoef et al.* (1999) noted that evaporation was important during the rainy season, but that its influence declined with the resumption of the Harmattan winds and the return of the dry season (see also *Gash et al.*, 1991, 1997). The marked reduction in downward longwave emission by the atmosphere during the dry season, contributing to efficient cooling of the surface by direct radiation to space, was found by *Frangi et al.* (1992) and *Verhoef et al.* (1999).

4 Surface Response To Subseasonal Variations in Atmospheric Constituents

Sunlight incident upon the surface varies with the slow, seasonal change of the solar zenith angle, but also as a result of fluctuations in atmospheric opacity due to clouds, water vapor, and aerosols, for example. These constituents shield the surface from incident solar radiation through reflection and absorption, while trapping longwave radiation and reëmitting it toward the surface (*Ramanathan et al.*, 1989; *Claquin et al.*, 1998). During one particularly strong dust outbreak over the AMF at Niamey during March 2006, the midday solar flux was reduced by 250 Wm^{-2} while downward atmospheric emission of longwave into the surface increased by 50 Wm^{-2} (*Slingo et al.*, 2006). In this section, we calculate the surface response to radiative forcing associated with subseasonal variations in atmospheric constituents, and compare the ability of the turbulent fluxes and longwave emission to regulate the temperature of the surface.

4.1 Calculation of Subseasonal Variations of Forcing

We calculate the surface radiative forcing by combining the net downwelling solar flux with the component of the downwelling longwave flux that is related to changes in atmospheric composition. This requires that we distinguish the contribution to the measured downwelling longwave by a change in composition from a change due to the response of the column to the forcing. Consider for example, an increase in aerosol optical thickness resulting from the passage of a dust plume. Absorption of radiation within the aerosol layer reduces the downwelling solar flux impinging on the surface, while increasing the downwelling flux of longwave (*Slingo et al.*, 2006). The downwelling longwave measured at the surface changes with the increase in atmospheric opacity and emission by the dust layer, along with changes in the emitting temperature. The forcing is the reduction of net solar radiation into the surface, offset by the increase in downwelling longwave due to the increase in opacity, while the change in downwelling longwave due to temperature changes is the forcing response. Thus, in order to infer the surface response to fluctuations in aerosol (or more generally

to variations in atmospheric composition), we need to distinguish the contributions to the measured downward longwave by the forcing and temperature response.

In a model, it is straightforward to calculate forcing by simply contrasting the radiative fluxes computed in the presence and absence of some constituent, while holding climate variables such as temperature fixed. Calculating the forcing from an observed atmospheric profile is complicated by the response of the observed temperature to the forcing. To separate the forcing and response contributions to the observed downward longwave flux, we regress this flux against surface air temperature and atmospheric constituents such as water vapor and aerosols. Then:

$$R'_{LW\downarrow}(0) = 4.82T'_s + 1.78q' + 16.7\tau'_A. \quad (1)$$

where $R'_{LW\downarrow}(0)$ is the fitted downward longwave at the surface in Wm^{-2} , T'_s is the surface air temperature in K measured by the eddy correlation instrument, q' is the column-integrated water vapor in mm measured by the radiosonde, and τ'_A is the (dimensionless) aerosol optical thickness. All quantities in (1) correspond to daily averages, and the prime symbols represents an anomaly relative to the 2006 calendar-year average. This decomposition assumes that temperature fluctuations are entirely in response to forcing. Dust outbreaks at Niamey are sometimes associated with the passage of a cold front (*Slingo et al.*, 2006) or gust front, both of which temporarily reduce temperature. In these cases, the temperature change and associated change in longwave fluxes are not strictly the result of the surface adjusting to local changes in atmospheric constituents. We will return to this point.

The measured downward longwave flux at the surface is shown in Fig. 3a, along with the fit by the regression model given by (1). In spite the simplicity of this empirical approach, the regression model accounts for over 97% of the observed variation in the downward longwave flux throughout the year. This percentage is stable throughout the year, and falls only to 93% if the regression model is restricted to the dry season (i.e. excluding May through October). While our regression model achieves this good fit without explicitly accounting for variations in clouds, variations in downward longwave due to clouds are implicitly accounted for in the regression model given the 0.41 correlation between water vapor and visible cloud optical thickness retrieved by ISCCP. The variance represented by (1) can be attributed approximately to the individual predictors, given that they are only weakly correlated. Column

water vapor (and associated changes in cloud optical thickness) account for nearly two-thirds of the downwelling longwave variance, with atmospheric temperature accounting for most of the rest.

The dependence of the regression model upon temperature, water vapor, and aerosol is consistent with linearized parameterizations of surface longwave described by *Fung et al.* (1984), where downward longwave into the surface increases with atmospheric emissivity (here represented by aerosol and water vapor) and atmospheric temperature. Because of vertical mixing, at least within the boundary layer during the dry season and within a deeper layer during the summer, surface air temperature T'_s is representative of variations in atmospheric temperature over a layer extending above the surface. We construct (1) to distinguish contributions to the measured downwelling longwave by changes in longwave opacity and the atmospheric temperature response. *Slingo et al.* (2008b) provide a physical interpretation of atmospheric longwave fluctuations measured during the ARM campaign at Niamey as a result of variations in temperature, moisture, and aerosol using a physically based formula by *Prata* (1996).

In response to a change in atmospheric composition and radiative forcing, the surface energy balance is:

$$\frac{\partial H}{\partial t} = F_{SW} + F_{LW} + \delta R_{LW} + \delta S_e + \delta(LE) \quad (2)$$

Here, H is the heat stored by the surface, and the solar and thermal components of the forcing are F_{SW} and F_{LW} , respectively. The response of the net longwave and turbulent fluxes to the forcing are given by δR_{LW} , δS_e and $\delta(LE)$, respectively, where δS_e is the anomalous sensible heat flux and $\delta(LE)$ is the anomalous latent heat flux.

To calculate the response of the surface fluxes (the terms prefixed by δ) to the forcing, we relate each term on the right side of (2) to a quantity measured at the Mobile Facility. For the solar forcing F_{SW} , we assign the anomalous net downward flux of solar radiation. This anomaly is computed by dividing out the slow modulation of the solar flux by the seasonal change in the daily average solar zenith angle, using the formula in Appendix A of *Hartman* (1994), and subtracting the long-term mean. The attribution of the measured solar flux entirely to forcing implicitly assumes that shortwave changes in response to the forcing

(e.g. through cloud cover) are comparatively small. For the longwave forcing, F_{LW} , we use the contribution to the observed downward longwave flux by variations in water vapor and aerosol optical thickness, as identified by the regression model (Fig. 3b). The time series of the surface longwave response δR_{LW} is given by the observed upward longwave emission (which depends upon the temperature of the surface) minus the temperature contribution to the observed downward longwave extracted using the regression model. The response of the turbulent fluxes is assumed to be given by the measured fluxes of sensible and latent heating. The forcing and response terms in (2) and their correspondence with measured quantities is summarized in Table 2.

The net surface forcing and response component of the downward longwave flux are illustrated in Figure 6 during March and April 2006 at the end of the dry season. The net shortwave anomaly due to changes in clouds, column water vapor, and aerosols is offset by the longwave effect of these constituents (Figure 6a). Three dust outbreaks can be seen as large reductions in the solar flux during March. The increased downwelling longwave is generally smaller in magnitude than the solar reduction, so that the total forcing has the sign of the solar flux but is smaller in magnitude. During the first dust outbreak in March, both the ground and air temperature are reduced by the passage of a cold front (*Slingo et al.*, 2006), which diminishes both the upwelling longwave measured at the surface and the component of downwelling longwave identified by (1) related to atmospheric temperature (Figure 6b). The two smaller dust events in late April, evident in the net downward solar in Figure 6a, are coincident with a rapid increase in column water vapor associated with a 'false start' to the monsoon (*Slingo et al.*, 2008a). During this time, elevated concentrations of dust and water vapor increase longwave emissivity, resulting in positive total forcing, while warming the surface air and ground, as can be inferred from Figure 6b.

The magnitude and characteristic time scale of variations in net surface forcing are shown in Figure 7. During the dry season, longwave forcing generally offsets and is slightly smaller than the solar contribution to the total (Figure 6a). However, at the height of the rainy season between July and September, the total forcing is dominated by the solar component, and uncorrelated with variations in longwave forcing (Figure 6b). According to Figure 3b,

the small longwave forcing is mainly the result of reduced variations in column water vapor. The marked increase in the variability of the total and solar forcing during the rainy season is related to the passage of African easterly waves (e.g. *Burpee, 1972*). This is indicated by the characteristic synoptic time scale in the spectrum of the solar forcing during this season. The spectrum is computed within a 42-day window centered at each date in Figure 7c. To emphasize frequencies longer than a day, the solar time series is filtered to remove frequencies shorter than 12 hours, and then subsampled every 6 hours to reduce aliasing. The total spectral power is normalized to be identical at each date to show how the dominant period (rather than the magnitude of variability) changes over time. Within the dry season, the spectrum is red, with the greatest power at longer periods. However, within the rainy season, periods of a few days dominate, representing synoptic variations in cloud cover associated with African waves modulated by the diurnal cycle of incident sunlight.

4.2 Surface Response to Subseasonal Forcing

How the surface responds to subseasonal variations in surface net radiative forcing is shown in Figure 8a. To calculate the response of the surface fluxes, we regress the net surface longwave response along with both the turbulent sensible and latent heat fluxes (each of the terms in eq. 2 prefixed by δ) with the net surface forcing (represented by the sum of the surface forcing $F_{SW} + F_{LW}$) as a predictor. To show how the response evolves throughout the year, the regression is computed within a four week period centered at each date. The largest regression coefficient on any date shows the predominate mechanism by which the forcing is balanced. The regression coefficients sum to unity when the forcing is completely compensated by these fluxes (as opposed to heat storage within the ground).

During the dry season, longwave emission and the turbulent sensible heat flux alternate as the dominant response to forcing variations (Figure 8a). Early in the rainy season, following the large monsoonal increase in column water vapor and atmospheric longwave opacity, the sensible heat flux has the greatest effect. The increased importance of the sensible heat flux soon after the arrival of the summer monsoon is presumably because the net surface longwave flux is limited by the increased longwave opacity of the monsoonal air, while soil

moisture remains too low to allow evaporation to compensate. However, by the height of this season in August and September, the evaporative flux increases and all three fluxes respond with nearly equal magnitude.

To focus upon the surface response to aerosol radiative forcing (as opposed to forcing by variations in water vapor and clouds), we repeat the regression calculation using the MFRSR AOT as the predictor. We perform the regression for March and April 2006 to see the response to the several significant dust events during this period. The surface response is shown in Figure 9. The surface radiative forcing by dust is balanced by roughly equal reductions in the turbulent flux of sensible heat into the atmosphere and the net upward longwave flux. The anomalous net upward longwave flux is negative because the surface cools more than the atmosphere. The large dust event in early March was related to the passage of a cold front (*Slingo et al.*, 2006), which cooled the ground and air. If the period of the regression calculation is extended through the end of June, when the atmospheric longwave opacity has been increased by the arrival of moist monsoon air, dust radiative forcing is balanced almost entirely by the sensible heat flux.

Figure 8b shows the regression of the individual upwelling longwave flux and downward response (proportional to air temperature) with respect to the net forcing. The net longwave flux stabilizes the ground temperature when the upwelling longwave is larger in magnitude than the downwelling response, which requires that the magnitude of the anomalous ground temperature exceed that of the surface air temperature anomaly. Between July and September, when rainfall is most frequent, fluctuations in air temperature are nearly zero, reflecting the steady delivery of moist, oceanic air during this season by the onshore monsoonal winds. During February and March, when net surface longwave most efficiently stabilizes the ground temperature against the forcing, the ground and air temperature anomalies are of opposite sign. Following the rainy season, the air and ground change temperature synchronously so the response of the net surface longwave to forcing is steady despite large changes in temperature. While it is unclear what controls the response of the ground-air temperature difference to forcing, this difference is crucial to the ability of the net surface longwave to stabilize the surface temperature.

The sensible heat flux also depends upon the ground-air temperature difference, according to its conventional parameterization (Arya, 1988):

$$S_e = C_p \rho C_D |w| (T_g - T_s), \quad (3)$$

where C_p is the heat capacity of the air at constant pressure, ρ is the air density, C_D is a coefficient that is generally parameterized in terms of atmospheric stability, w is the surface wind speed, T_g is the ground temperature, and T_s is the surface air temperature that appears in (1). We refer to the product $C_p \rho C_D |w|$ as the 'bulk coefficient' ω_0 . We calculate the bulk coefficient by dividing the sensible heat flux measured with the eddy correlation system by the ground-air temperature difference:

$$\omega_0 \equiv S_e / (T_g - T_s). \quad (4)$$

The ground temperature T_g is derived from broadband measurements of radiation upwelling from the surface, after applying a low-pass filter to remove frequencies higher than one hour, and resampling every 30 minutes to be consistent with the eddy correlation measurements. Equation 3 represents a parameterization of the sensible heat flux rather than a fundamental physical relationship. Nonetheless, 81% of variations in the daily averaged S_e during 2006 can be represented through its multiple regression with respect to the daily averaged ground-air temperature difference and the bulk coefficient averaged between 9h and 15h, the time of day when S_e is largest (Figure 5).

Because of the common influence of the ground-air temperature difference upon the sensible heat and net surface longwave fluxes, the comparative importance of S_e in stabilizing surface temperature might be explained in terms of variations in ω_0 . We regress the ground-air temperature difference and the bulk coefficient against the surface forcing to see if ω_0 is larger during periods when the sensible heat flux is a more effective regulator. The regression of $T_g - T_s$ and ω_0 with respect to the net forcing is shown in Figure 10. The regression is calculated within a four-week window centered at each date to show seasonal variations. In general, the seasonal evolution of the regression of ω_0 and the sensible heat flux with the forcing are similar (c.f. Figure 8a). In particular, the bulk coefficient is insensitive to the forcing during February and March of 2006 (and to a lesser extent during October and

November), when the sensible heat flux becomes inefficient compared to the net longwave response at compensating the forcing. However, during the remainder of the year, the ability of the sensible heat flux to regulate the ground temperature is augmented by the increase in the bulk coefficient by the forcing, and the comparatively large heat flux that results from a given ground-air temperature difference.

The bulk coefficient ω_0 varies with the surface wind speed and in a more complicated way upon the drag coefficient C_D . *Miller et al.* (2004a) describe how dust aerosols reduce ω_0 in an atmospheric general circulation model (AGCM). Negative forcing at the surface reduces the sensible heat flux, which powers mixing within a dry, continental boundary layer. A reduction in the vigor of boundary layer mixing transports less momentum to the surface, reducing ω_0 through its dependence upon the surface wind speed w . The direct reduction in eddy wind fluctuations has a similar effect. This is a positive feedback, because the reduction in the bulk coefficient causes a further reduction in the sensible heat flux. We are currently investigating whether this feedback between net forcing, the bulk coefficient, and the surface wind speed is evident in the AMF measurements. Another question that deserves investigation is why the sensitivity of the bulk coefficient to the forcing, apparent for most of the year in Figure 10, does not occur at certain times, such as February and March of 2006, when the net longwave flux is the most efficient mechanism at compensating the net surface forcing.

4.3 Contrasting Evaporative Response to Forcing During the Rainy Season

In contrast to the net longwave flux, the turbulent flux of latent heat shows almost no variation with forcing throughout the dry season (Figure 8a), consistent with the small seasonal average of this flux (Figure 5). Given sufficient moisture, latent heating can efficiently stabilize the temperature of the surface against fluctuations in solar radiation (*Pierrehumbert*, 1995). Over the tropical oceans, solar anomalies are typically balanced by evaporation (*Liu et al.*, 1994). At Niamey, only at the height of the rainy season in August does evaporation increase to compensate additional sunlight (Figure 8a). Earlier in the monsoon season, the

regression coefficient between the latent heat flux and solar heating is negative: evaporation actually decreases as sunlight increases. We interpret this anticorrelation as a consequence of limited soil moisture prior to significant rainfall. The clouds bringing the first rains early in the summer monsoon reduce the sunlight incident upon the surface. At the same time, the rainwater supplies moisture to the surface that is quickly depleted by evaporation within a few days. Thus, the anticorrelation results from the temporary availability of surface water for evaporation at the same time that the rain clouds shield the surface from sunlight. This is demonstrated in Figure 11, which shows that evaporation increases sharply with rainfall early in the monsoon season. Over the next few months, successive storms gradually refill the reservoir of soil moisture so that evaporation is no longer tied to a recent rain event. As the soil reservoir refills, solar radiation absorbed at the surface gradually replaces the availability of water as the factor controlling evaporation. By August, surface water is sufficiently abundant that evaporation is uncorrelated with precipitation (Figure 11). At this time, the latent heat flux is no longer limited by the supply of moisture and can buffer the surface from variations in sunlight, as indicated by the positive correlation (Figure 8a). Note that the regression between the solar flux and evaporation switches sign from negative to positive around the middle of July (Figure 8a), following a marked increase of the cumulative precipitation that represents a substantial fraction of the seasonal total (Fig. 2).

A temporary increase in evaporation following rainfall has been observed previously within the Sahel (*Wallace et al.*, 1993; *Allen and Grime*, 1995), although these studies found that evaporation and rainfall were coupled throughout the entire rainy season, rather than decorrelating with the accumulation of sufficient precipitation and soil moisture, indicated by the August values in Figure 11. If the soil surface inhibits the penetration of rainwater, then runoff may increase after a storm at the expense of accumulation and storage within the soil. We do not know whether the evaporative fluxes measured at the Niamey AMF originate where rainwater penetrates into the soil and is stored, creating a reservoir that eventually allows evaporation to respond to variations in sunlight.

During 2006, there was little additional rainfall after mid-September (Fig. 2). By November, the latent heat flux returned to near zero, indicating that the moisture supplied to the

upper soil layer during the rainy season had been depleted. Although 2005, the year prior to the ARM campaign, was unusually wet (*Slingo et al.*, 2008a), the latent heat flux was found to be small by late November 2005, when the measurements began (Figure 4).

5 Conclusions

We have described the seasonal contrast in the surface energy balance at a site within the Sahel, using measurements of radiative and turbulent fluxes at the ARM Mobile Facility stationed at Niamey, Niger throughout 2006. The measurement site is a continental location, with rainfall restricted to the southwesterly phase of the West African monsoon, when surface winds bring moist air onshore from the tropical Atlantic Ocean. The direction of the surface wind determines how solar heating is balanced by the land surface at Niamey, in contrast to the tropical oceans where the surface energy balance is roughly uniform throughout the year. During the dry season, solar heating is balanced predominately by longwave radiation and the turbulent flux of sensible heat. Only at the height of the rainy season is evaporation of comparable importance in balancing sunlight.

The surface energy balance at Niamey shows a sharp seasonal contrast for two reasons. First, soil moisture is available for evaporation only after the start of the rainy season, in contrast to oceanic or even vegetated regions where evapotranspiration can supply moisture to the atmosphere throughout the year. Early in the rainy season, evaporation increases temporarily following the occurrence of precipitation, which replenishes moisture at the surface against evaporative loss. Sufficient accumulation of soil moisture by the height of the rainy season allows evaporation to decorrelate with the supply of moisture from recent precipitation events, and correlate instead with the flux demanded by solar heating of the surface. It has been suggested that moisture storage within the Sahel can increase the persistence of multi-year wet periods (*Nicholson, 2000; Koster et al., 2004*). While an unusually large amount of rain fell during the summer prior to the measurement campaign (*Slingo et al., 2008a*), the latent heat flux was virtually zero in 2006 until a few months after the arrival of the monsoon. That the latent heat flux remained negligible during the dry season and initial phase of the summer monsoon, despite anomalously large rainfall the prior year, suggests that any stored moisture cannot be easily accessed by the surface layer. However, plants reëmerging with the annual resumption of the rains may extend their roots deep enough to tap the stored moisture and make rainfall available to the surface that accumulated during a prior year. The observed restriction of significant evaporation to the height of the rainy

season at Niamey also suggests that dimming of the surface by aerosols weakens the hydrologic cycle only during this season (*Miller and Tegen, 1998; Ramanathan et al., 2001*), and that the hydrologic cycle is decorrelated from aerosol forcing at other times of the year.

The sharp seasonal contrast in the surface energy balance is also related to the annual change in longwave opacity associated with the seasonal reversal of the wind direction associated with the monsoon. With the arrival of relatively cool, moist air from the Atlantic Ocean, the column moisture increases threefold. The arrival of this moisture in late April increases the absorption of longwave radiation emitted by the surface, redirecting some of it downwards, reducing the ability of surface to cool through longwave radiation. In contrast, during the dry season between November and April, the mean winds are from the Sahara desert to the north and the column is relatively transparent in the longwave. During this season, solar radiation absorbed at the surface is balanced predominately by longwave emission, and the turbulent flux of sensible heat is generally of secondary importance in compensating solar heating of the surface. However, after the increase in atmospheric longwave opacity associated with the arrival of the southwesterly monsoon, and before significant rainfall, the sensible heat flux is the predominate offset to solar heating. At the height of the rainy season, when the reservoir of soil moisture has been replenished, the evaporative flux is of comparable importance to the sensible and net longwave fluxes.

In general, how the surface balances the time-averaged solar heating varies with seasonal changes in atmospheric water vapor, which modulates the greenhouse effect and the ability of the surface to radiate thermal energy directly to space. Radiative forcing of the surface also results from more rapid, subseasonal variations in atmospheric constituents like water vapor, clouds, and aerosols. On these shorter time scales, the net longwave response and the turbulent flux of sensible heat alternate in their ability to regulate the surface temperature, except at the height of the rainy season when evaporation has a comparable effect. The efficacy of the sensible heat flux S_e depends dynamical feedbacks within the atmospheric boundary layer. During most of the year, the bulk coefficient ω_0 relating S_e to the ground-air temperature difference $T_g - T_s$ decreases with negative forcing associated with an increase in aerosol or water vapor concentration. This is a positive feedback because a decrease in ω_0

further reduces the sensible heat flux in response to the surface forcing for a given $T_g - T_s$. During the dry season, the efficiency with which S_e compensates the forcing compared to the longwave response varies with the ability of the forcing to change ω_0 . When ω_0 is insensitive to the forcing, as during February and March of 2006, the longwave response is the predominate compensator of the forcing.

This raises the question of how the forcing alters ω_0 . In AGCM experiments (*Miller et al.*, 2004a), the forcing changes the turbulent flux of sensible heat from the surface to the atmosphere that drives mixing within dry continental boundary layers, and thus the transfer of momentum to the surface. This alters ω_0 through its dependence upon surface wind speed. Alternatively, surface radiative forcing at the Niamey AMF may change ω_0 through the coefficient C_D which depends upon atmospheric stability. We are currently investigating the mechanism relating the forcing to the bulk coefficient ω_0 , along with why this sensitivity is sometimes absent. However, the more general point is that the response of surface fluxes to surface radiative forcing by variations in the concentration of atmospheric constituents depends upon feedbacks involving boundary layer dynamics. The boundary layer response to surface radiative forcing can ultimately feed back upon atmospheric constituents such as dust whose entrance into the atmosphere depends upon the surface wind speed. Negative radiative forcing beneath an aerosol layer, which reduces boundary layer mixing and the surface wind speed, is believed to limit the magnitude of dust storms on Mars (*Newman et al.*, 2002). While local dust sources around Niamey are believed to make a secondary contribution to the local aerosol optical thickness, measurements of the turbulent and radiative fluxes by the AMF may reveal how aerosol radiative forcing alters the boundary layer and the surface wind in more productive sources upwind.

Acknowledgments: Data were obtained from the Atmospheric Radiation Measurement (ARM) Program sponsored by the U.S. Department of Energy, Office of Science, Office of Biological and Environmental Research, Environmental Sciences Division. We thank Nazim Bharmal, Chris Bishop, Brian Cairns, Anthony Del Genio, Hamidou Hama, Randall Koster, Issa Lélé, Sally McFarlane, Mark Miller, Sharon Nicholson, Chris Taylor, and Peng Xian. We also thank Didier Tanré for aerosol retrievals from the AERONET site at Banizoumbou,

Niger. This work was supported by the Climate Dynamics Program of the National Science Foundation through ATM-06-20066

Appendix

In this appendix, we show that the overlap of rainy days identified by the ARM Mobile Facility optical instrument and the operational rain gauge is unlikely to result from chance, indicating that both instruments have skill at detecting rainfall, despite disagreement.

By analogy, consider N distinct items and select n of them. After replacement, select m items and calculate the probability that k were selected both times. Here N could represent the total number of days during the rainy season, while n and m are the number of rainy days identified by the airport rain gauge and the AMF optical instrument, respectively. We want to know if the k rainy days in common between the two instruments are likely to result merely from random chance, indicating that one or both of the instruments has no skill at detecting rainfall.

The probability that the first item selected in the second round was also chosen in the first round is $\frac{n}{N}$. Similarly, the probability that the first two items of the second round were selected in the first round is $\frac{n}{N} \frac{n-1}{N-1}$. In general, the probability $p_{k,m-k}$ that the first k items in the second round were chosen in the first round, while the subsequent $m-k$ items were not is:

$$p_{k,m-k}(N, n, m, k) = \left(\frac{n}{N}\right) \left(\frac{n-1}{N-1}\right) \cdots \left(\frac{n-k+1}{N-k+1}\right) \left(\frac{N-n}{N-k}\right) \left(\frac{N-n-1}{N-k-1}\right) \cdots \left(\frac{N-n-(m-k)+1}{N-m+1}\right) \quad (5)$$

The first row of (5) gives the probability of the first k items from the second round being in common with those chosen during the first. The second row gives the probability of the remaining $m-k$ items being unique to the second round. If the k repeated and $m-k$ new items were chosen during the second round in a different order, then the numerators and denominators in (5) would simply be rearranged, so that the sequence would have the same probability $p_{k,m-k}(N, n, m, k)$. There are $\binom{m}{k}$ ways for the k common days to be selected among the total m during the second round, and each has equal probability. Thus, the total probability of selecting k days in common is:

$$p(N, n, m, k) = \binom{m}{k} p_{k,m-k}(N, n, m, k) \quad (6)$$

which we can rewrite as:

$$p(N, n, m, k) = \frac{m!n!(N-n)!(N-m)!}{k!(m-k)!(n-k)!(N+k-m-n)!N!} \quad (7)$$

As a check, we have confirmed numerically that

$$\sum_{k=0}^m p(N, n, m, k) = 1, \quad (8)$$

for several combinations of N , n , m , and k . Also, the probability is the same when n and m are reversed, as expected by symmetry.

Setting N equal to 180 (roughly the number of days in the rainy season), with n and m equal to 57 and 52 as identified by the airport rain gauge and optical instrument, then random chance would result in between 9 and 24 common days 99% of the time (Figure 12). In fact, the two instruments have 39 days in common and as many as 45 if storms around midnight assigned to successive days by the two instruments are included. According to Figure 12, this overlap is very unlikely, and suggests that despite the deposition of dust aerosol on the optical instrument, it remained sensitive to the occurrence of rain.

References

- Allen, S. J., and V. Grime (1995), Measurements of transpiration from savannah shrubs using sap flow gauges, *Agric. Forest Meteorol.*, *75*, 23–41.
- Arya, S. P. (1988), *Introduction to Micrometeorology, Int. Geophys. Ser.*, vol. 42, Academic Press, San Diego, 307 pp.
- Burpee, R. W. (1972), The origin and structure of easterly waves in the lower troposphere of North Africa, *J. Atmos. Sci.*, *29*, 77–90.
- Claquin, T., M. Schulz, Y. Balkanski, and O. Boucher (1998), Uncertainties in assessing radiative forcing by mineral dust, *Tellus*, *50B*, 491–505.
- Coakley, J. A., and R. D. Cess (1985), Response of the NCAR Community Climate Model to the radiative forcing by the naturally occurring tropospheric aerosol, *J. Atmos. Sci.*, *42*, 1677–1692.
- Emanuel, K. A. (1994), *Atmospheric Convection*, Oxford University Press, 580 pp.
- Fouquart, Y., B. Bonnell, G. Brogniez, J. C. Buriez, L. Smith, J. J. Morcrette, and A. Cerf (1987), Observations of Saharan aerosols: Results of ECLATS field experiment, II, Broad-band radiative characteristics of the aerosols and vertical radiative flux divergence, *J. Clim. Appl. Meteorol.*, *26*, 38–52.
- Frangi, J. P., A. Druilhet, P. Durand, H. Ide, J. P. Pages, and A. Tinga (1992), Energy budget of the Sahelian surface-layer, *Ann. Geophysicae*, *10*, 25–33.
- Fung, I. Y., D. E. Harrison, and A. A. Lacis (1984), On the variability of the net longwave radiation at the ocean surface, *Rev. Geophys. Space Phys.*, *22*, 177–193.
- Gash, J., J. Wallace, C. Lloyd, A. Dolman, M. Sivakumar, and C. Renard (1991), Measurements of evaporation from fallow sahelian savannah at the start of the dry season, *Q. J. R. Met. Soc.*, *117*, 749–760.

- Gash, J., P. Kabat, B. Monteny, M. Amadou, P. Bessemoulin, H. Billing, E. Blyth, H. De-Bruin, J. Elbers, T. Friberg, G. Harrison, and C. Holwill (1997), The variability of evaporation during the hapex-sahel intensive observation period., *J. Hydrol.*, *188-189*, 385–399.
- Geerts, B., and T. Dejene (2005), Regional and diurnal variability of the vertical structure of precipitation systems in Africa based on spaceborne radar data, *J. Climate*, *18*, 893–916.
- Guedalia, D., C. Estournel, and R. Vehil (1984), Effects of Sahel dust layers upon nocturnal cooling of the atmosphere (ECLATS experiment), *J. Clim. Appl. Meteorol.*, *23*, 644–650.
- Hartman, D. L. (1994), *Global Physical Climatology*, Academic Press, New York, 411p.
- Hastenrath, S., and P. Lamb (1977), Some aspects of circulation and climate over the eastern equatorial Atlantic, *Mon. Weather Rev.*, *105*, 1019–1023.
- Huffman, G., R. Adler, P. Arkin, A. Chang, R. Ferraro, A. Gruber, J. Janowiak, A. McNab, B. Rudolph, and U. Schneider (1997), The Global Precipitation Climatology Project (GPCP) combined precipitation dataset, *Bull. Amer. Meteorol. Soc.*, *78*, 5–20.
- Johnson, B., B. Heese, S. McFarlane, P. Chazette, A. Jones, N. Bellouin, S. Osborne, and J. Haywood (2008), Vertical distribution and radiative forcing of mineral dust and biomass-burning aerosols over West Africa during DABEX, *J. Geophys. Res.*, (in preparation).
- Kiehl, J. T., and K. E. Trenberth (1997), Earth’s annual global mean energy budget, *Bull. Amer. Meteorol. Soc.*, *78*, 197–208.
- Koster, R. D., P. A. Dirmeyer, Z. Guo, G. Bonan, E. Chan, P. Cox, C. T. Gordon, S. Kanae, E. Kowalczyk, D. Lawrence, P. Liu, C.-H. Lu, S. Malyshev, B. McAvaney, K. Mitchell, D. Mocko, T. Oki, K. Oleson, A. Pitman, Y. C. Sud, C. M. Taylor, D. Verseghy, R. Vasic, Y. Xue, and T. Yamada (2004), Regions of strong coupling between soil moisture and precipitation, *Science*, *305*, 1138–1140, doi:10.1126/science.1100217.
- Liu, W. T., A. Zhang, and J. K. B. Bishop (1994), Evaporation and solar irradiance as regulators of sea surface temperature in annual and interannual changes, *J. Geophys. Res.*, *99(C6)*, 12,623–12,638.

- McFarlane, S. A., E. Kassianov, J. Barnard, C. Flynn, and T. P. Ackerman (2008), Surface shortwave aerosol radiative forcing during the ARM Mobile Facility deployment in Niamey, Niger, *J. Geophys. Res.*, (submitted).
- Miller, M. A., and A. Slingo (2007), The Atmospheric Radiation Measurement (ARM) Mobile Facility (AMF), and its first international deployment: Measuring radiative flux divergence in West Africa, *Bull. Amer. Meteorol. Soc.*
- Miller, R. L., and I. Tegen (1998), Climate response to soil dust aerosols, *J. Climate*, *11*, 3247–3267.
- Miller, R. L., J. Perlwitz, and I. Tegen (2004a), Feedback by dust radiative forcing upon dust emission through the planetary boundary layer, *J. Geophys. Res.*, *109*(D24), D24209, doi:10.1029/2004JD004912.
- Miller, R. L., I. Tegen, and J. Perlwitz (2004b), Surface radiative forcing by soil dust aerosols and the hydrologic cycle, *J. Geophys. Res.*, *109*, D04203, doi:10.1029/2003JD004085.
- Newman, C. E., S. R. Lewis, and P. L. Read (2002), Modeling the Martian dust cycle, 1, Representations of dust transport processes, *J. Geophys. Res.*, *107*(E12), 5123, doi:10.1029/2002JE001910.
- Nicholson, S. (2000), Land surface processes and Sahel climate, *Rev. Geophys.*, *38*, 117–139.
- Nicholson, S. E., and J. P. Grist (2003), The seasonal evolution of the atmospheric circulation over West Africa and Equatorial Africa, *J. Climate*, *16*, 1013–1030.
- Pierrehumbert, R. T. (1995), Thermostats, radiator fins, and the runaway greenhouse, *J. Atmos. Sci.*, *52*, 1784–1806.
- Prata, A. J. (1996), A new long-wave formula for estimating downward clear-sky radiation at the surface, *Q. J. R. Met. Soc.*, *122*, 1127–1151, doi:10.1256/smsqj.53305.
- Ramanathan, V., R. D. Cess, E. F. Harrison, P. Minnis, B. R. Barkstrom, E. Ahmad, and D. L. Hartmann (1989), Cloud-radiative forcing and climate: Results from the Earth Radiation Budget Experiment, *Science*, *243*, 57–63.

- Ramanathan, V., P. J. Crutzen, J. T. Kiehl, and D. Rosenfeld (2001), Aerosols, climate, and the hydrologic cycle, *Science*, *294*, 2119–2124.
- Ravel, A., and V. Ramanathan (1989), Observational determination of the greenhouse effect, *Nature*, *342*, 758–761.
- Rossow, W., and E. Duenas (2004), The International Satellite Cloud Climatology Project (ISCCP) web site: An online resource for research, *Bull. Amer. Meteorol. Soc.*, *85*, 167–172, doi:10.1175/BAMS-85-2-167.
- Simpson, J. J., J. S. Berg, C. J. Koblinsky, G. L. Hufford, and B. Beckley (2001), The NVAP global water vapor dataset: Independent cross-comparison and multiyear variability, *Remote Sens. Environ.*, *76*, 112–129.
- Slingo, A., T. P. Ackerman, R. P. Allan, E. I. Kassianov, S. A. McFarlane, G. J. Robinson, J. C. Barnard, M. A. Miller, J. E. Harries, J. E. Russell, and S. Dewitte (2006), Observations of the impact of a major Saharan dust storm on the atmospheric radiation balance, *Geophys. Res. Lett.*, *33*, L24817, doi:10.1029/2006GL027869.
- Slingo, A., N. Bharmal, G. Robinson, J. Settle, R. Allan, H. White, P. Lamb, M. I. Lélé, D. Turner, S. McFarlane, E. Kassianov, J. Barnard, C. Flynn, and M. Miller (2008a), Overview of observations from the RADAGAST experiment in Niamey, Niger. Part 1: Meteorology and thermodynamic variables, *J. Geophys. Res.*, (submitted).
- Slingo, A., H. E. White, N. A. Bharmal, and G. J. Robinson (2008b), Overview of observations from the radagast experiment in niamey, niger. part 2: Radiative fluxes and divergences, *J. Geophys. Res.*, (submitted).
- Verhoef, A., S. J. Allen, and C. R. Lloyd (1999), Seasonal variation. of surface energy balance over two Sahelian surfaces, *Int. J. Climatol.*, *19*, 1267–1277.
- Wallace, J., L. C.R., and S. M.V.K. (1993), Measurement of soil, plant and total evaporation from millet in Niger, *Agric. For. Meteorol.*, *63*, 149–169.

Table 1: Summary of analyzed measurements. ‘Data Stream’ refers to the name of the data stream at the ARM data archive: <http://www.archive.arm.gov>. ‘Variable Name’ is the netcdf name of the variable in the daily data stream file. ISCCP is the International Satellite Cloud Climatology Project.

Measured Quantity	Data Stream	Variable Name	Dates Available	Resolution
<i>Broadband Radiative Fluxes</i>				
Downwelling Shortwave	skyrad60s	down_short_hemisp	26 Nov 05 – 7 Jan 07	1 min.
Downwelling Longwave	skyrad60s	down_long_hemisp_shaded1	26 Nov 05 – 7 Jan 07	1 min.
Upwelling Shortwave	gndrad60s	up_short_hemisp	24 Nov 05 – 7 Jan 07	1 min.
Upwelling Longwave	gndrad60s	up_long_hemisp	24 Nov 05 – 7 Jan 07	1 min.
<i>Turbulent Fluxes</i>				
Latent Heat Flux	30ecor	lv_e	26 Nov 05 – 7 Jan 07	30 min
Sensible Heat Flux	30ecor	h	26 Nov 05 – 7 Jan 07	30 min
<i>Atmospheric Opacity</i>				
Sonde Column Water Vapor	sondewnpn	dp	7 Jan 06 - 7 Jan 07	6 hr.
MFRSR AOT	-	-	25 Nov 07 – 7 Jan 07	20 sec.
ISCCP Cloud Optical Thickness	-	-	1 Nov 05 – 31 Dec 06	3 hr.
<i>Meteorological Quantities</i>				
Surface Air Temperature	30ecor	mean_t	26 Nov 05 – 7 Jan 07	30 min
Surface Specific Humidity	30ecor	mr	26 Nov 05 – 7 Jan 07	30 min
Rainfall	met	precip_rate_mean	6 Jan 06 - 7 Jan 07	1 min.

Table 2: Surface forcing and response terms in (2) and their correspondence with measured variables. All quantities are daily averages and anomalies relative to the long-term mean. q' is column water vapor from radiosondes; τ'_A is aerosol optical thickness retrieved from MFRSR radiances; T'_s is surface air temperature from the eddy correlation instrument.

Symbol	Variable	Measured Quantity
F_{SW}	Solar Forcing	Downwelling minus Upwelling Shortwave
F_{LW}	Longwave Forcing	$1.78 q' + 16.7 \tau'_A$
δR_{LW}	Net Longwave Response	Upwelling Longwave minus $4.82 T'_s$
δS_e	Sensible Heat Response	Sensible Heat Flux
$\delta(L E)$	Latent Heat Response	Latent Heat Flux

Figures

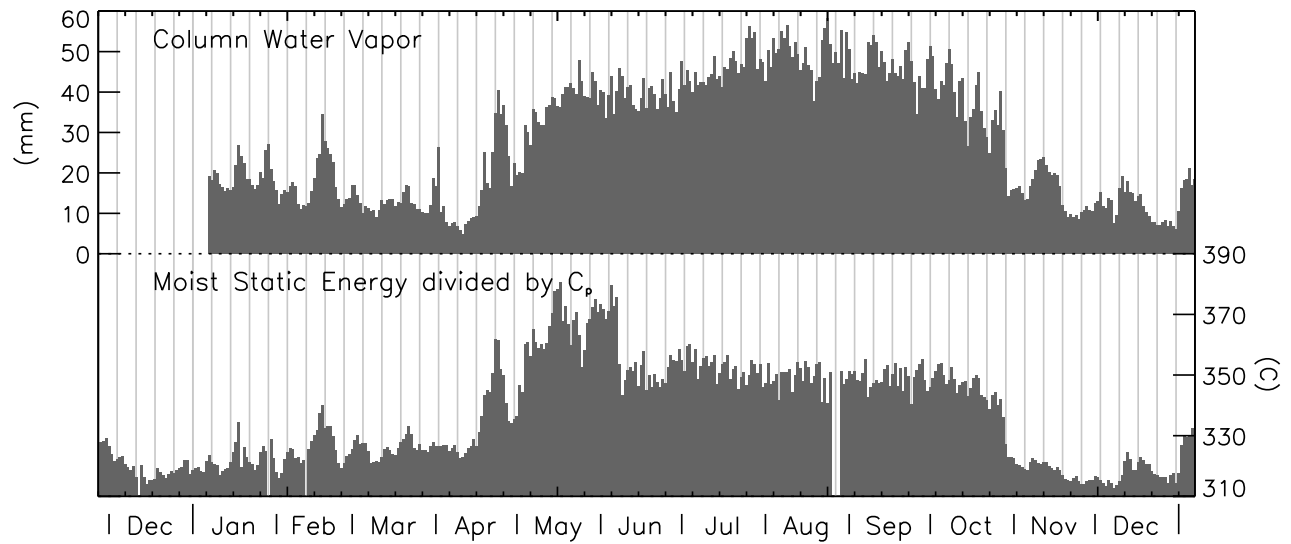


Figure 1: a) Column-integrated radiosonde water vapor (mm) and b) moist static energy (divided by C_p to have units of K) measured at the ARM Mobile Facility at Niamey, Niger. Light gray vertical lines are spaced seven days apart, beginning on 1 January 2006.

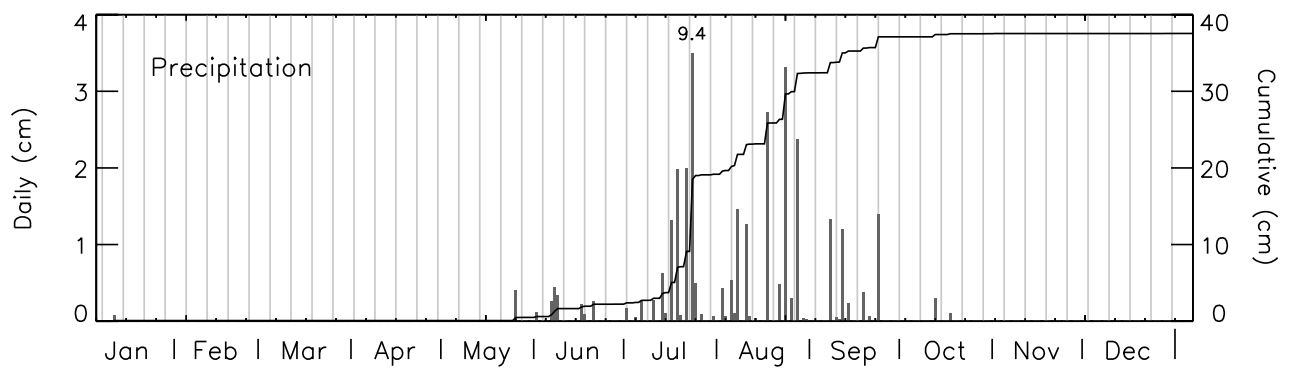


Figure 2: Daily (gray) and cumulative (black) rainfall in cm, measured at the ARM Mobile Facility in Niamey, Niger. Daily rainfall measured by the optical instrument on 24 July 2006 was off the scale at 9.4 cm. Light gray vertical lines are spaced seven days apart, beginning on 1 January 2006. Rainfall was not measured between 13 May and 26 May, but no rainfall was recorded at another site in Niamey (*Slingo et al.*, 2008a).

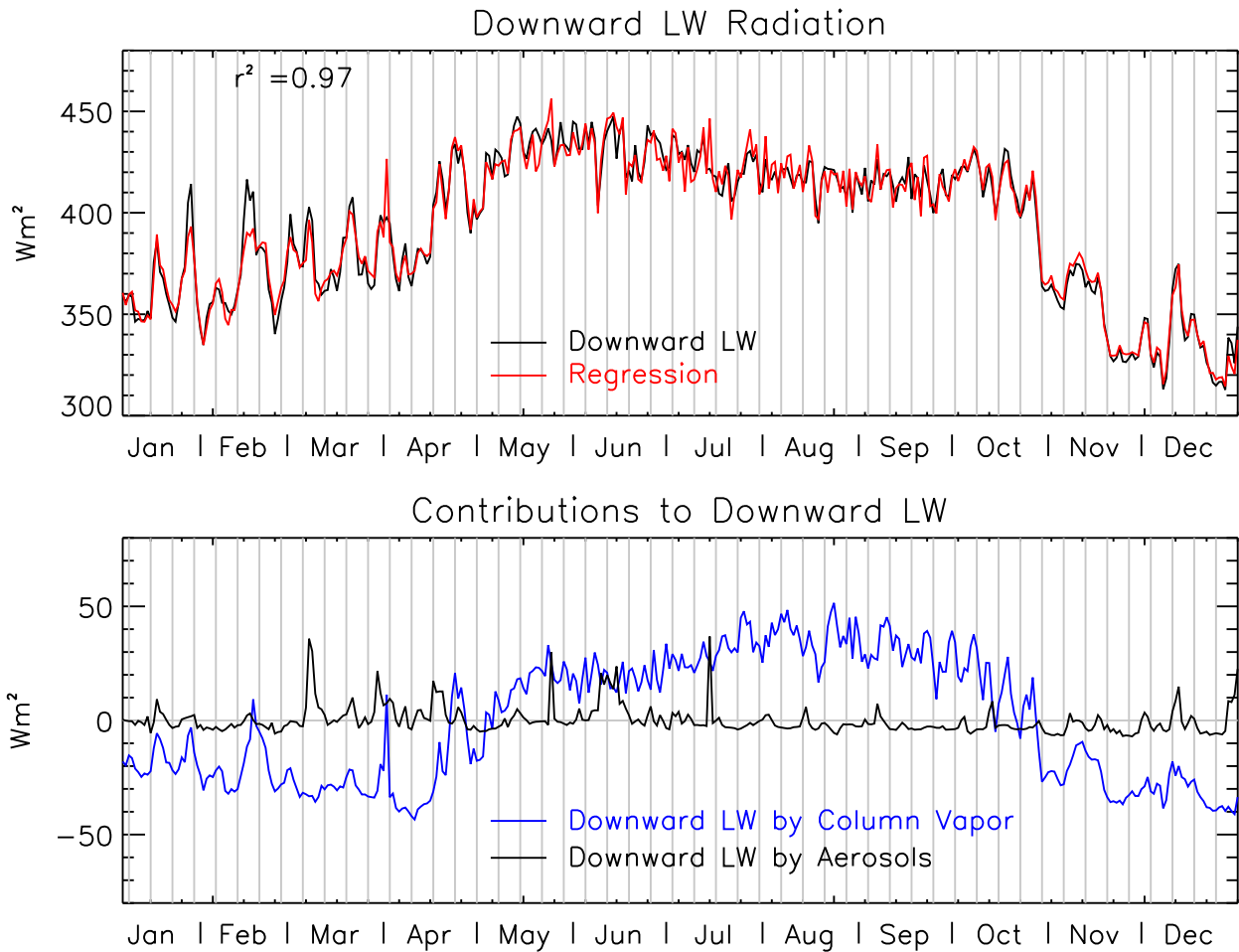


Figure 3: a) Daily averaged downward flux of longwave radiation measured at the ARM Mobile Facility (black, Wm^{-2}), versus the downward flux constructed by multiple regression with respect to surface air temperature, column water vapor, and aerosol optical thickness (red). The regression model represents 97% of the measured variations of the daily downward flux. b) Contributions to downward longwave at the surface (Wm^{-2}) by water vapor (blue) and aerosol optical thickness (black) according to the regression model. Vertical gray lines are spaced seven days apart, beginning on 1 January 2006. *Add the uncertainty for each coefficient to the caption.*

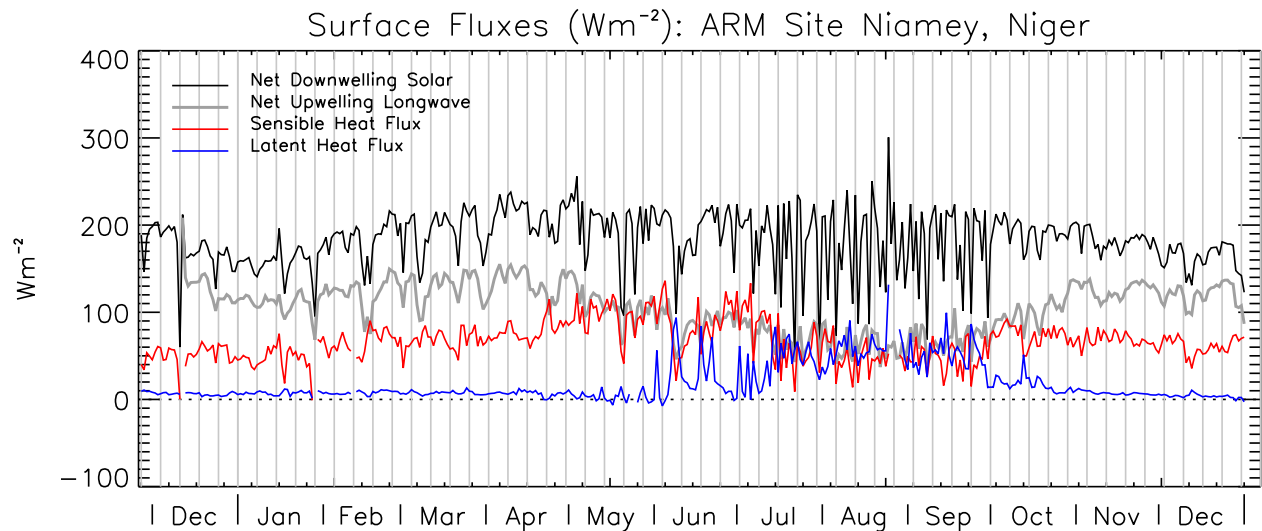


Figure 4: Daily averaged surface fluxes (Wm^{-2}) measured at the ARM Mobile Facility at Niamey, Niger. Vertical gray lines are spaced seven days apart, beginning on 1 January 2006.

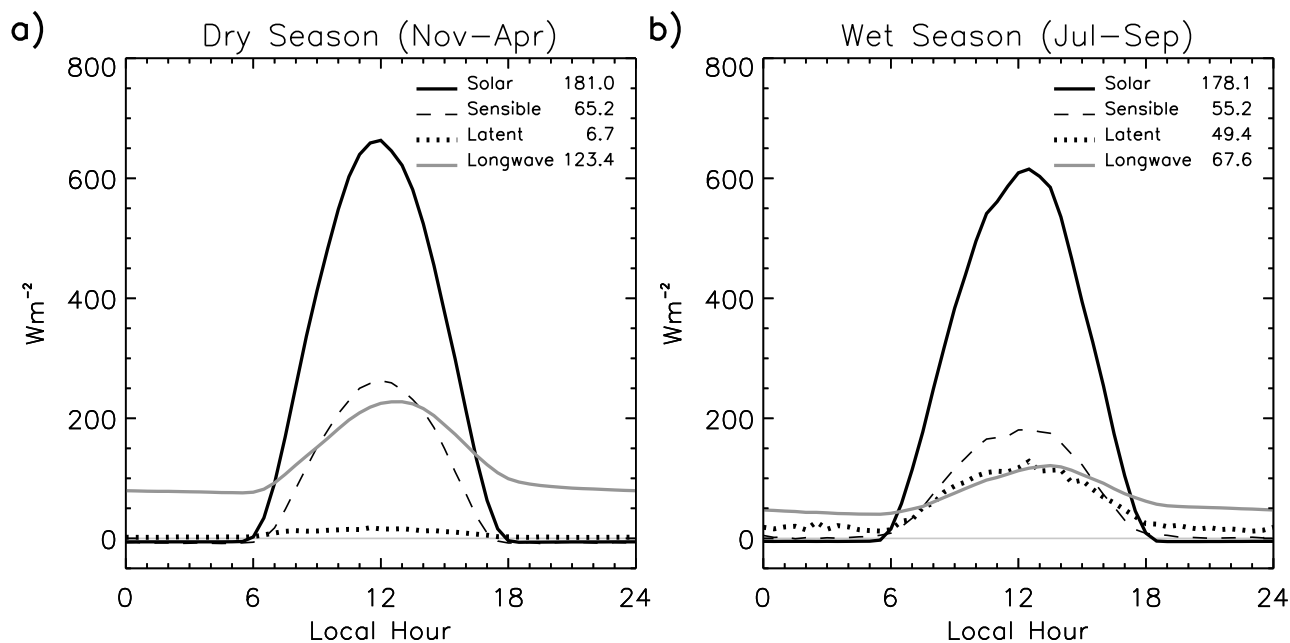


Figure 5: Diurnal cycle of surface fluxes (Wm^{-2}) during the a) dry season (November–April), and b) the height of the wet season (July–September), measured at the ARM Mobile Facility at Niamey, Niger. Diurnal averages of each flux are listed at the upper right corner. Radiative fluxes were subsampled every thirty minutes (after filtering periods shorter than sixty minutes to reduce aliasing) to be consistent with the resolution of the turbulent fluxes.

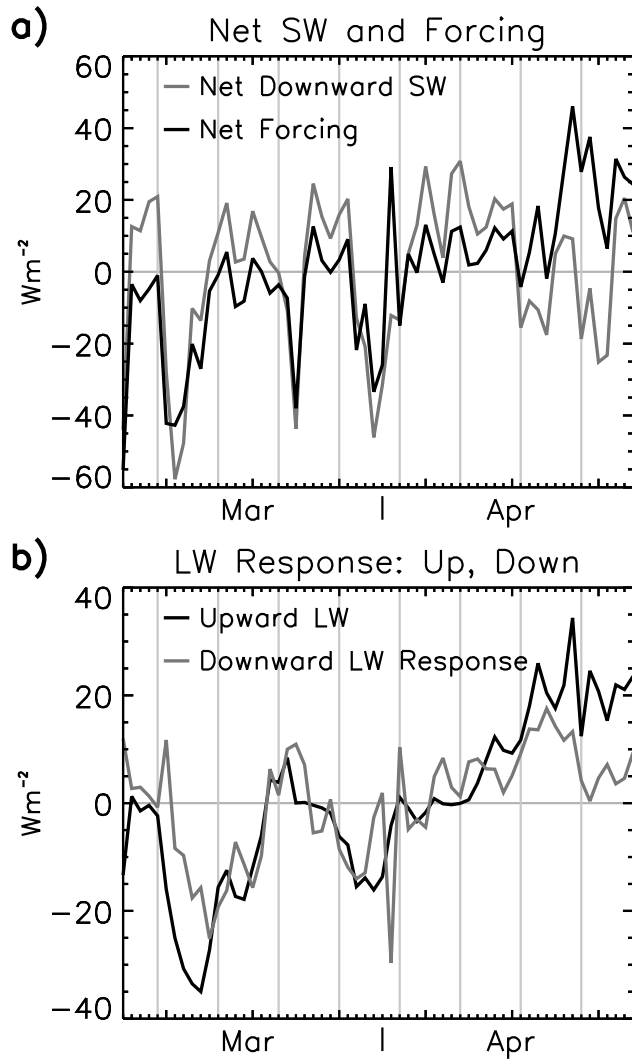


Figure 6: Daily averaged a) net (downwelling minus upwelling) shortwave along with net forcing equal to net shortwave plus downwelling longwave due to changes in column water vapor and dust aerosol, and b) Downwelling longwave associated with changes in atmospheric temperature, and upwelling longwave. All quantities are measured in Wm^{-2} (or calculated through regression with measured quantities) during March and April 2006 at the ARM Mobile Facility in Niamey, Niger. Vertical gray lines are spaced seven days apart, beginning on 1 January 2006.

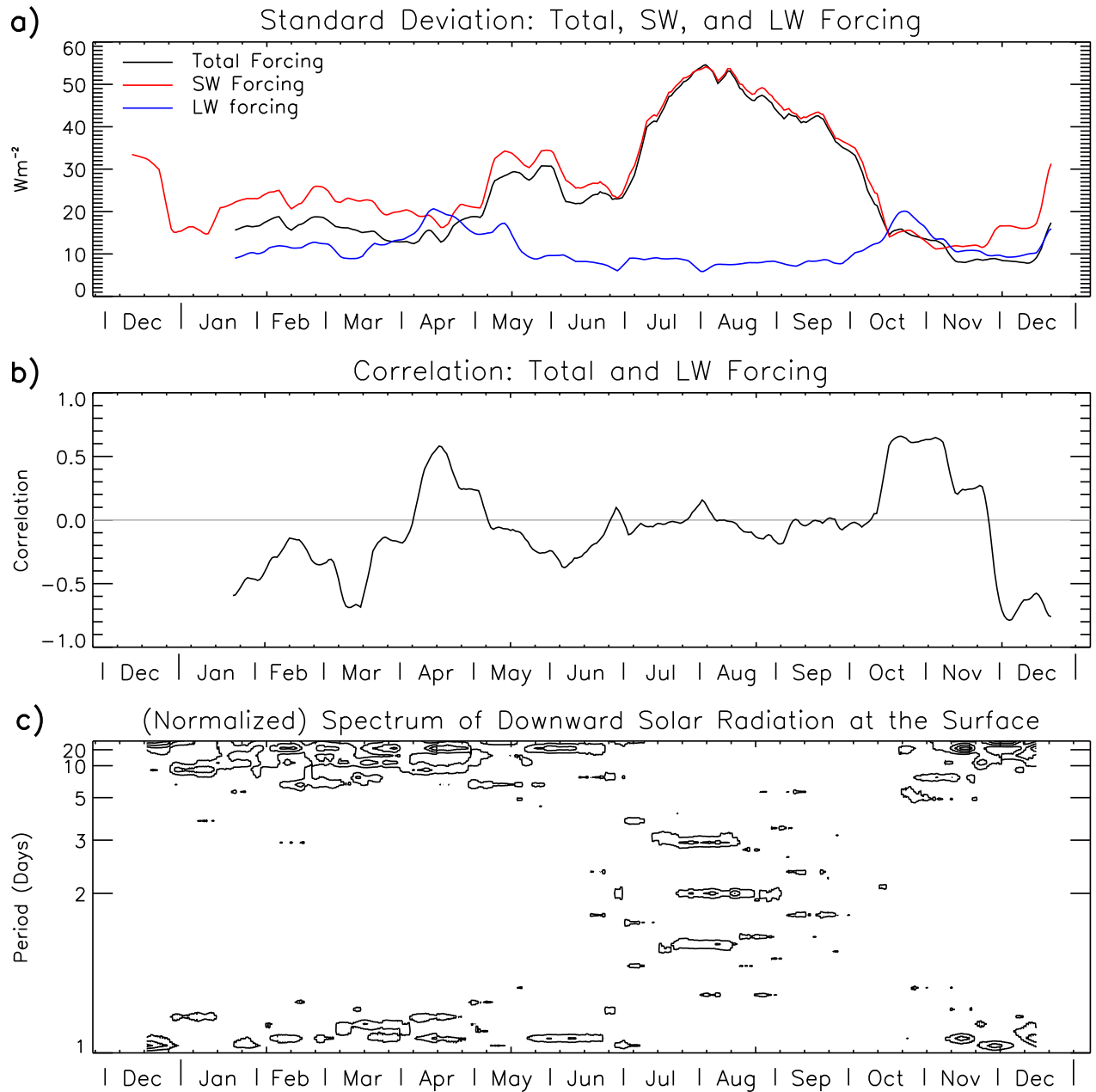
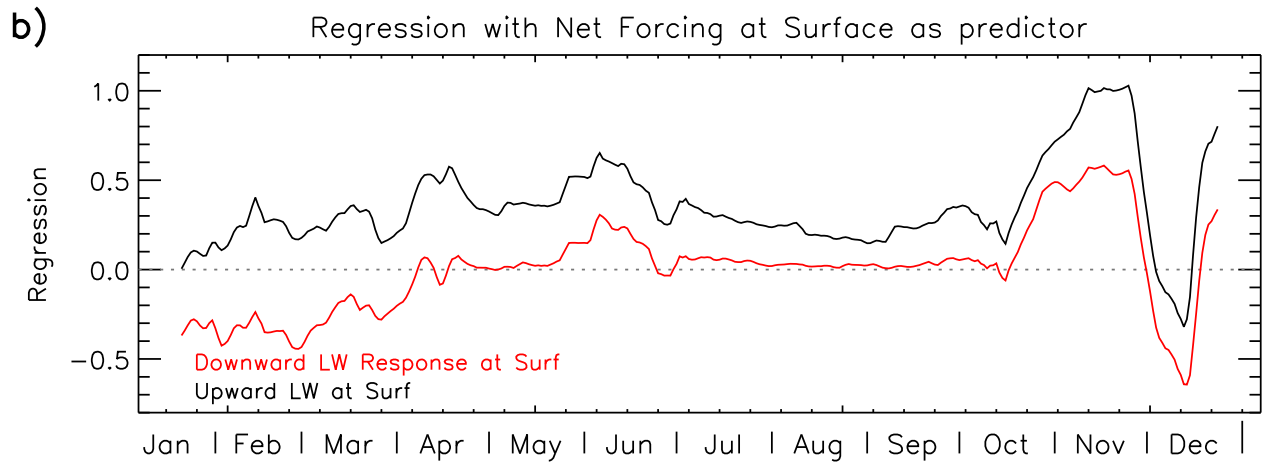
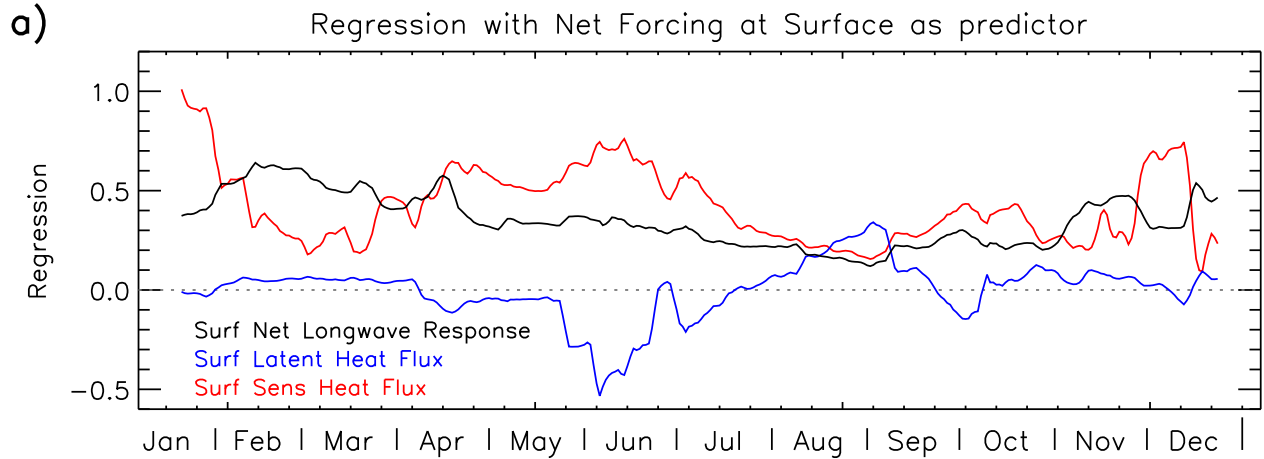


Figure 7: a) Standard deviation of total along with solar and longwave forcing in Wm^{-2} , b) correlation of total and longwave forcing, c) spectrum of downward solar radiation at the surface. All quantities are computed as a function of time within a 44-day window centered at each date. The diurnal cycle within each period is subtracted prior to calculation. The spectrum is normalized to have the same frequency-integrated power at each date.



~/Documents/mystuff/programs/arm/correlation/pro/surfForcing_regress_wrt_t.pro

Figure 8: Regression of surface fluxes with respect to the net surface forcing over the ARM Mobile Facility at Niamey, Niger. For each date, the regression is calculated using measurements ranging from two prior to two weeks after. The diurnal cycle within this period is subtracted prior to calculation of the covariance. Regression of forcing versus a) the net longwave response and turbulent fluxes, and b) individual components of the net longwave response: upward longwave and downward longwave related to atmospheric temperature.

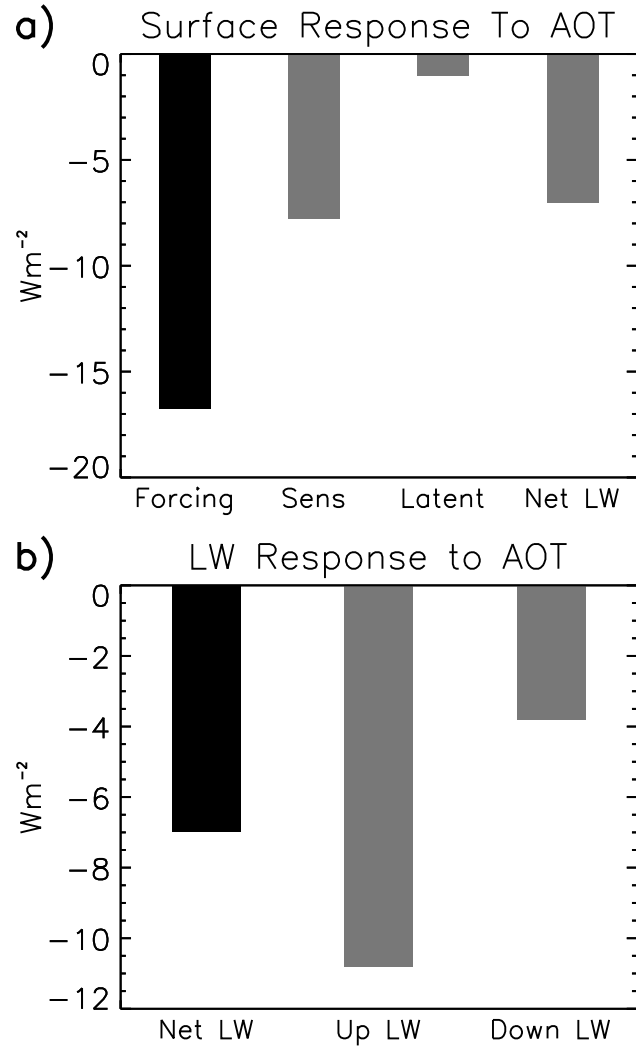


Figure 9: Regression of surface fluxes with respect to MFRSR AOT measured at the ARM Mobile Facility at Niamey, Niger. The regression is calculated using measurements during March and April 2006, when there were several large dust events. The standard deviation of AOT during this period is 0.46. The diurnal cycle within this period is subtracted prior to calculation of the covariance. Regression of AOT versus a) dust radiation forcing at the surface, along with the turbulent fluxes and net longwave response, and b) individual components of the net longwave response: upward longwave and downward longwave related to atmospheric temperature.

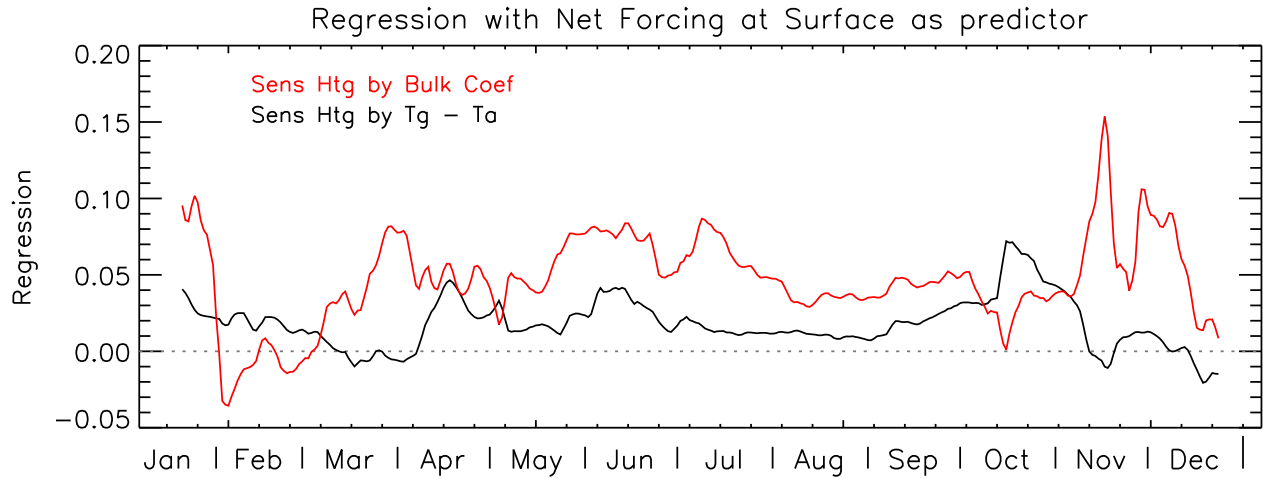


Figure 10: Regression of the ground-air temperature difference and the inferred bulk coefficient with respect to the net surface forcing over the ARM Mobile Facility at Niamey, Niger. For each date, the regression is calculated using measurements ranging from two prior to two weeks after. The diurnal cycle within this period is subtracted prior to calculation of the covariance.

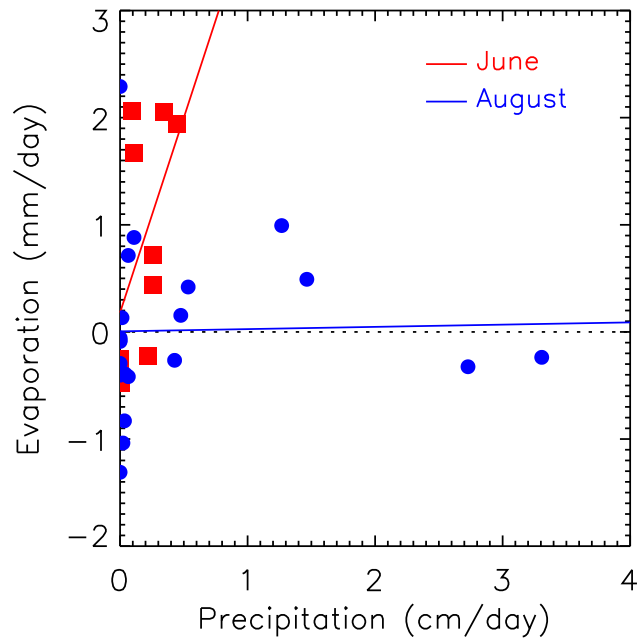


Figure 11: Relation between daily averaged precipitation and anomalous evaporation (for days with precipitation) during June and August, the early and peak wet season at the ARM Mobile Facility at Niamey, Niger. Evaporation anomalies are computed relative to the preceding week.

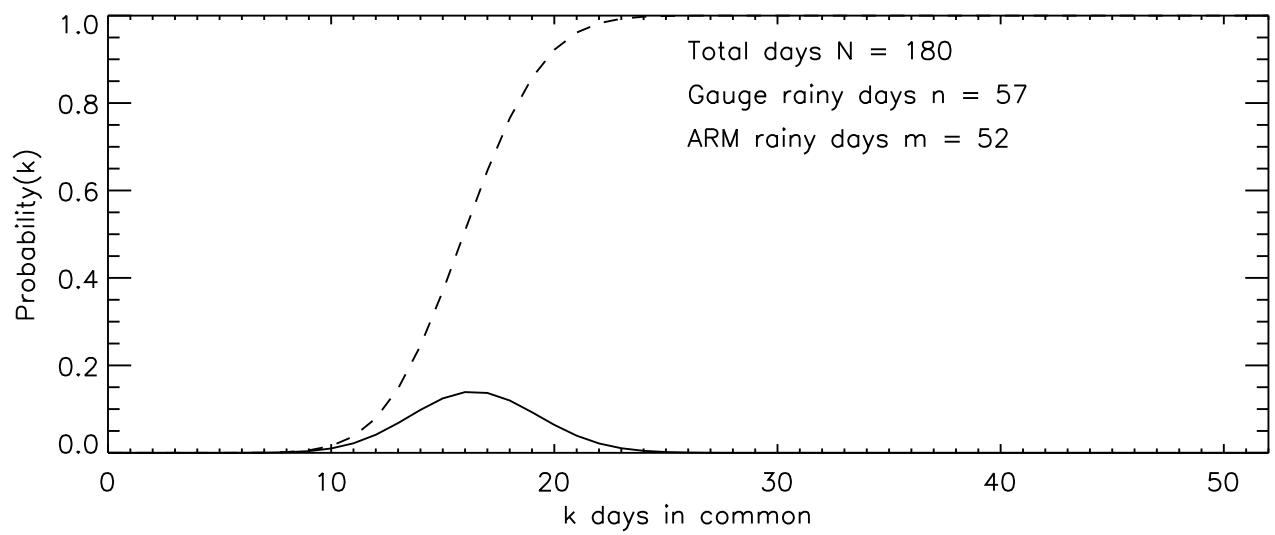


Figure 12: Probability (solid) and cumulative probability (dashed) of the 57 days identified by the airport rain gauge and the 52 days identified by the AMF optical instrument having k days in common if one or both instruments have no skill in identifying rainy days.